# Insights into the mechanism of diurnal variations in methane emission from the stem surfaces of *Alnus japonica*

Kenshi Takahashi[*,1)], Ayaka Sakabe[*,2,3)] Wakana A. Azuma[*,4)], Masayuki Itoh[5)], Tomoya Imai[1)], Yasuki Matsumura[1)], Makiko Tateishi[3)], Yoshiko Kosugi[3)]

1) Research Institute for Sustainable Humanosphere, Kyoto University, Gokasho, Uji 611-0011, Japan
2) The Hakubi Center, Kyoto University, Yoshida-honmachi, Sakyo-ku, Kyoto 606-8501, Japan
3) Graduate School of Agriculture, Kyoto University, Kitashirakawa Oiwake-cho, Sakyo-ku, Kyoto 606-8502, Japan
4) Graduate School of Agricultural Science, Kobe University, Kobe 657-8501, Japan
5) School of Human Science and Environment, University of Hyogo, Himeji 670-0092, Japan

* These authors contributed equally to this work.

**Corresponding authors**

Kenshi Takahashi (ORCID ID: 0000-0002-5905-2708)
Phone: +81-774-38-3862, E-mail: takahashi.kenshi.2v@kyoto-u.ac.jp
Ayaka Sakabe (ORCID ID: 0000-0002-1447-7710)
Phone: +81-75-753-6086, E-mail: sakabe.ayaka.4a@kyoto-u.ac.jp
Wakana A. Azuma (ORCID ID: 0000-0002-4254-719X)
Phone: +81-78-803-5936, E-mail: wakana@port.kobe-u.ac.jp

ORCID ID for co-authors
Masayuki Itoh: 0000-0002-7070-616X

Tomoya Imai: 0000-0001-7026-0287

Yasuki Matsumura: 0000-0003-1228-2693

Makiko Tateishi: 0000-0002-0507-1372

Yoshiko Kosugi: 0000-0002-0256-8404

**Brief heading (< 93 characters)**

Diurnal amplitudes in stem $CH_4$ emissions are season-dependent.

**Summary**

- Recent studies have suggested that in certain environments, tree stems emit methane ($CH_4$). This study explored the mechanism of $CH_4$ emission from the stem surfaces of *Alnus japonica* in a riparian wetland. Stem $CH_4$ emission rates and sap flux were monitored year-round, and fine-root anatomy was investigated.
- $CH_4$ emission rates were estimated using a closed-chamber method. Sap flux was measured using Granier-type thermal dissipation probes. Root anatomy was studied using both optical and cryo-scanning electron microscopy.
- $CH_4$ emissions during the leafy season exhibited a diurnally changing component superimposed upon an underlying continuum in which the diurnal variation was in phase with sap flux. We propose a model in which stem $CH_4$ emission involves at least two processes: a sap flux–dependent component responsible for the diurnal changes, and a sap flux–independent component responsible for the background continuum. The contribution ratios of the two processes are season–dependent.
- The background continuum possibly resulted from the diffusive transport of gaseous $CH_4$ from the roots to the upper trunk. Root anatomy analysis indicated that the intercellular space of the cortex and empty xylem cells in fine roots could serve as a passageway for transport of gaseous $CH_4$.

**Key words**: methane flux, stem, diurnal variations, sap flux, *Alnus japonica*, fine-root, anatomy, optical and cryo-SEM images

## Introduction

Atmospheric methane ($CH_4$) is an important greenhouse gas; therefore, the identification of its source and its quantification are crucial issues in addressing climate change. The global $CH_4$ budget remains highly uncertain because of the diversity of biogenic and abiotic $CH_4$ sources and emission

processes, reduction by chemical reaction with the short-lived hydroxyl radical, and lack of observations of sources and sinks (Saunois et al., 2020). Wetland $CH_4$ emissions are recognized as the largest natural source in the global $CH_4$ budget, contributing to roughly one third of total natural and anthropogenic emissions. However the estimated $CH_4$ emission strengths are still highly uncertain (Kirschke et al., 2013), clearly indicating that there is a need for improved estimates.

In recent years, emission of $CH_4$ from the stems of living and dead trees has drawn considerable attention as a potentially important new source of atmospheric $CH_4$ (Carmichael et al., 2014, 2018, Barba et al., 2019a; Covey and Megonigal, 2019). Findings of experimental studies have increasingly suggested that tree-mediated processes can contribute significantly as a pathway of $CH_4$ emission in wetland ecosystems (Terazawa et al., 2007, Gauci et al., 2010; Pangala et al., 2015, Pangala et al, 2017, Terazawa et al., 2021). Even in upland forest ecosystems in which surface soils under aerobic conditions are generally considered to act as $CH_4$ sinks, emission of $CH_4$ from tree stems may diminish the capacity of surface soils to take up $CH_4$ (Pitz and Megonigal, 2017, Pitz et al., 2018). However, the understanding of the mechanisms by which $CH_4$ is emitted from the stems of living trees remains ambiguous. For example, it is unclear whether trees function as passive "pipes" through which $CH_4$ is transported diffusively from the rhizosphere to the atmosphere, whether they serve as pipes in which xylem flow transports $CH_4$ in the dissolved state, or whether living trees produce $CH_4$ in the heartwood (Covey et al., 2012, Barba et al., 2019a). A unique application of $^{222}Rn$ gas in a recent study by Megonigal et al. (2020) enabled to them investigate the mechanism for gas transport through trees of three species of *Fagus grandifolia* Ehrh., *Liriodendron tulipfera* L., and *Quercus rubra* L. Their suggested mechanism is based on the fact that transpiration lowers stem water content. Transpiration draws water out from water-filled intercellular spaces in the xylem, reducing the tortuosity of diffusion pathways, and thereby increasing methane diffusion rates. Aside from soil and heartwood production of $CH_4$, methane-oxidizing bacteria have recently been identified within tree bark (*Melaleuca quinquenervia*) and sapwood (*Populus* sp.), which may be able to affect $CH_4$ emissions from trees (Jeffrey et al., 2021a; Feng et al. 2022). In addition, under conditions where tree stems are waterlogged,

transport of gaseous $CH_4$ through the bark has been reported for *M. quinquenervia* that features a distinctive bark that is thick, layered, spongy, paper-like, shaggy and peeling bark (Jeffrey et al., 2020).

The aim of the present study was to elucidate the mechanisms of $CH_4$ transport inside wetland trees. Our group has been investigating the process by which $CH_4$ is emitted from the stems of *Alnus japonica* (Thunb.) Steud. trees growing in a riparian wetland with a monsoon climate. We recently reported $CH_4$ emission rates and seasonal variations dependent on individual trees based on year-round measurements using a closed-chamber method coupled with near-infrared laser spectrometry for *in situ* $CH_4$ detection (Sakabe et al., 2021). The rates of $CH_4$ emission from the stems of *A. japonica* trees exhibited maxima in summer and minima in winter, and this pattern was closely related to the methanogenic activity in the soil, as demonstrated by path analysis. In addition, our results indicated that intensive rainfall could modulate the rates of $CH_4$ emission, as transient rainfall-associated changes in the soil environment, such as fluctuations in groundwater level, could affect the rates of $CH_4$ emission. In the present study, hourly based measurements conducted throughout the year enabled us to examine the diurnal properties of $CH_4$ emission rates in detail. We discuss the possible processes giving rise to diurnal variation in the rates of $CH_4$ emission from the stem surfaces of *A. japonica*, especially in terms of the relation between the $CH_4$ emission rates and sap flux. A diurnal feature of stem $CH_4$ flux was clearly observed in *L. tulipifera* L in an upland forest (Pitz and Megonigal, 2017), but their data were limited to only three days. They briefly discussed the need to study the relationship between diurnal variations in $CH_4$ flux and sap flow. Thereafter, sap flux has been shown to associate with temporal $CH_4$ emissions at diurnal and seasonal scales (Barba et al., 2019b; Jeffrey et al., 2020). Sap flux occurs when water in the soil is absorbed by the roots and ascends via the transpiration of leaves; this system connects the underground to the aboveground parts through the inside of trees. Attention has also been focused on the relation between the day-night variations in $CH_4$ flux and air temperature (Barba et al., 2019b; Jeffrey et al., 2020). By contrast, other studies have found no clear evidence of diurnal variations in $CH_4$ emissions (Pangala et al., 2014; Terazawa et al., 2015; Schindler et al., 2021). In the present study, we conducted a detailed examination of the relationship between the

properties of diurnal $CH_4$ emission and the results of sap flux measurements.

In addition, in order to explore the mechanistic insights into stem $CH_4$ emissions in the present study, samples of fine roots were collected and observed using optical and cryo–scanning electron microscopy (cryo-SEM). Previous optical microscopy studies have indicated that the pathway for gas exchange between the roots and aboveground environment is composed of the aerenchyma, a type of tissue comprising a relatively high proportion of spaces or lacunae (Evert 2006; Takahashi et al., 2014). The function and formation of lysigenous aerenchyma have been well studied, particularly in roots of rice and maize. These structures, which are formed by cell death and subsequent lysis, provide oxygen from shoots to root, enabling the plant to tolerate anaerobic conditions (Drew et al., 2000; Yamauchi et al., 2013). Distinct root aerenchymas have also been observed in mature mangrove trees, the proportion of which expands from the root apex (Purnobasuki & Suzuki, 2004). The other tissue, called secondary aerenchyma, is a white sponge tissue formed in the stem, hypocotyl, tap root, adventitious roots, and root nodules of some leguminous, herbaceous, and woody plants, which plays a role in flood tolerance (Stevens et al., 2002; Verboven et al., 2012; Yamauchi et al., 2013). In addition to the characteristics of these specific tissues that can be examined using optical microscopy, cryo-SEM can provide unique information regarding the distribution of water in the observed tissue at a given point in time (e.g., Webb et al., 1986; Azuma et al., 2016). Using these tools to examine the root tissues of *A. japonica* could help elucidate the mechanisms by which $CH_4$ is transported in fine roots, either in the gaseous form or dissolved in sap flow. Here, we report the identification of intercellular spaces that could function as conduits for transporting $CH_4$ molecules in the gaseous state.

## Materials and methods

### *Measurements of stem $CH_4$ emission and sap flux*

The experimental design and the target wetland for *in situ* measurements of $CH_4$ flux from the stem surfaces of *A. japonica* was the same as that described in our recent paper (Sakabe et al., 2021); thus, only a brief description will be given here. Measurements were conducted in a temperate

coniferous forest in the Kiryu Experimental Watershed (KEW, 34°58′N, 136°00′E) in Shiga Prefecture, which is located in central Japan. The detailed site description including a topographic map has been provided elsewhere (Kogusi et al., 2007; Itoh et al., 2007; Sakabe et al., 2016, 2021). The elevation range of the study site is 190 – 255 m. The forest comprises 60-year-old Japanese cypress trees (*Chamaecyparis obtusa* Sieb. et Zucc.) that were planted in 1959. Some riparian wetlands were located upstream of check dams that were constructed across the main stream of the watershed approximately 100 years ago.. The dominant tree species in the wetland is *A. japonica*. Three mature *A. japonica* trees growing naturally in the riparian wetland were selected for this study (hereafter: Trees 1, 2, and 3). The height and diameter at breast height of Trees 1, 2, and 3 were 11.3 m and 12.7 cm, 8.3 m and 8.9 cm, and 12.2 m and 10.8 cm, respectively. The trunks of *A. japonica* trees were not waterlogged at all. Surface soil around the trees may be saturated with water for a few hours during and after extreme heavy rainfall..

Stem $CH_4$ flux was measured using a dynamic closed-chamber system, in which a laser-based instrument (FGGA907-0010, Los Gatos Research, CA, USA) was employed for interference-free, real-time monitoring of gaseous $CH_4$ concentrations at atmospheric levels. The span of the laser spectrometer was calibrated against standard gas containing atmospheric levels of $CH_4$ diluted in synthetic air (Koatsu Gas Kogyo Co., Ltd., Osaka, Japan). A chamber that enclosed the whole stem circumference was attached to each tree. Each chamber consisted of a custom-made cylinder made of clear acrylic resin (25 cm outer diameter × 30 cm high) and was equipped with an inlet and outlet connected to the laser-based analyzer via PFA tubes (4.25 mm inner diameter). The chambers were attached to the stem surface at a specific height to cover all directions, and remained in place throughout the observation period. The height with respect to the bottom of the chamber ranged from 30 to 50 cm above the ground surface. The chambers were usually ventilated using ambient air. The target chamber system was temporally closed for 10 min during measurements, and the air from the chamber was circulated using a diaphragm pump. The sample air flow was circulated at a constant flow rate of 1.5 L $min^{-1}$, which was regulated using a mass flow controller (MPC0005BBRN010000,

azbil, Tokyo, Japan). Sequential switching among the chambers was regulated using solenoid valves (CKD-CD16AC, Campbell Scientific, UT, USA). The sampled air was pre-dried using a gas dryer (PD-50T-24MPS, Perma Pure Inc., NJ, USA). A portion of the circulating sample air was introduced into the laser spectrometer to measure the concentrations of $CH_4$ and residual water vapor. The $CH_4$ concentrations were corrected for water vapor dilution. The stem $CH_4$ flux per stem surface area (nmol $m^{-2}$ $s^{-1}$) was deduced from the temporal changes in gas concentration using the following equation:

$$Flux = \frac{dc}{dt} \times \frac{V}{S} \times \rho$$

where dc/dt represents the slope of the linear regression of the temporal change in gas concentration *c* (ppm) at time *t* (s) during chamber closure, *V* represents the volume of the chamber headspace, *S* represents the surface area of the stem, and ρ represents the air mole density (mol $m^{-3}$). In our study, *S* was determined based on geometric measurements, and the bark of *A. japonica* characteristically exhibits small, shallow cracks. The flux data from each of the three chambers were obtained hourly. All flux values determined in this study were positive, which means that net emission of $CH_4$ occurred throughout the year. The $CH_4$ fluxes were accepted with a condition that the determination coefficient of linear regression was larger than 0.90. The flux data discarded were 0.3, 0.5, and 0.3 % of the raw data of measurements for Tree 1, 2, and 3, respectively. Based on the root mean square error of the linear regression within the measurements, the minimum detection limits for $CH_4$ flux were 0.04, 0.07, and 0.04 nmol $m^{-2}$ $s^{-1}$ for Trees 1, 2, and 3, respectively, for the 6-min chamber deployment period.

Sap flux was measured for each tree every 30 min using the thermal dissipation method and Granier-type sensors (Granier, 1987). Sap flux was measured using the same method reported by Tateishi et al. (2008). Each sensor consisted of a pair of thermocouple probes (a heater probe and a reference probe) 20 mm in length and 2 mm in diameter. The probes were inserted vertically into the sapwood (150-mm apart, 0-20 mm depth). All sensors were installed on the north-facing side of the trunk and covered to avoid exposure to direct sunlight. The upper heater probe was continually supplied with a power of 0.2 W. The heat generated by the heater probe dissipated into the sapwood

and the vertical sap flow surrounding the probe. The temperature difference between the heater and reference probes (ΔT) was converted to the sap flux per cross-sectional area of the sapwood at the heater probe ($cm^3\ m^{-2}\ s^{-1}$) as reported by Granier (1987). ΔT values were measured every second, and all values averaged over 30 min were recorded using a CR-1000 data logger (Campbell Scientific, USA). The highest temperature difference was defined as the zero-flux condition for each day.

Environmental parameters including air temperature, rainfall, and short-wave radiation in the KEW were measured as described in previous studies (Kosugi et al., 2007; Sakabe et al. 2016, 2021). The average annual air temperature was 13.7°C, and the average annual rainfall between 2010 and 2019 was 1,799 mm. The amount of rainfall was measured using a tipping bucket rain gauge (RT-5, Ikeda Keiki, Japan). This paper analyses the observation data of $CH_4$ flux, sap flux and environmental parameters between September in 2017 and August in 2018.

***Optical microscopy and cryo-SEM***

To elucidate the pathway of $CH_4$ transport in plant tissue from the soil, fine roots ($n = 6$) were carefully collected from approximately 5-cm depth of soil close to the study trees and then flash frozen *in situ* in liquid nitrogen. The frozen fine roots were then cut from the individual trees, sealed in plastic tubes, transported to the laboratory under a large amount of dry ice, and stored at −80°C until analysis. To observe the anatomic characteristics of the fine roots without dehydrating the tissues, which would alter the water status at the time of collection, transverse sectionswere observed using cryo-SEM (SU8230, Hitachi, Japan). Secondary electron images were obtained at an accelerating voltage of 3 kV with shallow sublimation. To examine the fine root anatomy in detail, some fine roots were sealed in plastic bags before flash freezing and transported to the laboratory. Transverse sections (26 μm thickness) of these fine roots were prepared and double stained with safranin–fast green. The sections were then observed under an optical microscope (Eclipse 80i, Nikon, Tokyo) and photographed using a digital camera (E-620, Olympus, Tokyo). Fine root samples examined by cryo-SEM were also sectioned transversely and photographed under the optical microscope, as described above.

The potential for sublimation of moisture from frozen fine root tissues during transport from the field to the laboratory or during storage in a freezer raises concerns regarding artifacts that may appear on cryo-SEM images. To determine whether any such artifacts were present in the above observations, the samples were compared with those prepared in an experiment using an *A. japonica* sapling grown in the laboratory under well-watered conditions (tree height = 83 cm). In this experiment, fine roots of the sapling (n = 3) were observed under cryo-SEM using the same procedure described above, with the exceptions of sample transport from the field to the laboratory and storage in a freezer. That is, in the sapling experiment, cryo-SEM was conducted immediately after the samples were flash frozen, as this condition is unlikely to introduce artifacts. Comparison of the cryo-SEM images of the sapling experiments (Fig. S1) confirmed that no artifacts were present in the images of the samples collected at the study site.

## Results

### *Diurnal properties of stem $CH_4$ flux and model of the emission mechanism*

Figure 1 shows the stem $CH_4$ fluxes from three *A. japonica* trees in different seasons, along with the air temperature, rainfall, downward short-wave radiation, and sap flux. Flux measurements with a high time resolution of one hour revealed the existence of diurnal changes that were superimposed over the background continuum. Stem $CH_4$ emissions peaked about an hour after noon in the afternoon in all three trees. In addition, the daytime increase in $CH_4$ emission was almost synchronous with the increase in sap flow. Intriguingly, declines in sap flux due to rainfall or cloudy weather were related to a decline in the magnitude of the daytime increase in $CH_4$ emissions (Fig. 1A), suggesting that the diurnal amplitude in $CH_4$ emissions depends on sap flux. We note that measurements of the stem $CH_4$ fluxes and sap flux were conducted between September in 2017 and August in 2018, of which such diurnal features were evident only during leafy season. Another feature to be addressed here is that the *total* $CH_4$ emission rates exhibited overall decreasing and increasing trends in autumn and summer, respectively. This is due to the seasonal variation in $CH_4$ emissions, in

242 which they differed by up to about two orders of magnitude between the minima in February-March
243 during defoliation and the maxima in August of leafy season (Sakabe et al., 2021). Similarly, as
244 reported previously, relative differences in sap flux between autumn and summer were due to its
245 seasonality in which the sap fluxes kept quite low during defoliation and began to increase with the
246 spread of leaves in April, and decreased gradually after the summertime maxima as the season
247 progressed.

248 Figure 2 shows the monthly average stem $CH_4$ and sap fluxes for the three study trees over the
249 periods September to November 2017 and May to July 2018. The $CH_4$ emission peaks were almost
250 synchronous with the sap flux peaks. In calculating the monthly averages, data for periods when the
251 rainfall amount over the previous 24 h exceeded 10 mm were excluded. Intense rainfall events were
252 associated with transient increases in stem $CH_4$ emissions, and these increases were typically triggered
253 within a few hours of the start of the intense rainfall event and then gradually faded over the course of
254 several days (Fig. 1A). This phenomenon will be associated with the dynamic response to rainfall of
255 the vertical distributions of gaseous and dissolved $CH_4$ concentrations in subsurface soil layers, as
256 discussed in our recent paper (Sakabe et al., 2021). The data in Figure 2 show that the diurnal amplitude
257 of $CH_4$ emissions declined with the progression from autumn to winter, along with a seasonal decrease
258 in sap flux, whereas the diurnal amplitude increased with the progression from spring to summer. It
259 should be noted that no diurnal component of $CH_4$ emissions could be detected from late autumn to
260 early spring, although emission of $CH_4$ could be clearly detected even in winter, as we recently reported
261 (Sakabe et al., 2021). At the study site, *A. japonica* trees drop their leaves in late November, and begin
262 to leaf in April. In addition, a careful look at Fig. 2 shows that, in Tree 3, the diurnal peaks in stem
263 $CH_4$ emission and sap flux appeared about an hour later than those in Tree 1 and 2. This may be due
264 to the fact that the study trees grow in a shallow valley, which causes individual differences in the time
265 of sunlight exposure. Sap flow is linked to leaf transpiration, and leaf transpiration is linked to sunlight
266 exposure.

267 We make an attempt to separate the $CH_4$ flux data into two components, namely, diurnally

varying and unvarying components, based on their comparison with the sap flux data. The diurnal patterns of stem $CH_4$ and sap fluxes were found to be almost in phase with each other, which allows us to infer that there could be a process associated with sap flow. Accordingly, we will henceforth refer to the diurnally varying component as the "sap flux-dependent" component, whereas the diurnally unvarying component as the "sap flux-independent" component. We note that, however, using the terms of "sap flux-dependent" and "sap flux-independent" does not negate any $CH_4$ transporting process driven by other than sap flow. Possible $CH_4$ transport mechanisms regulating the stem $CH_4$ emissions from the stem surface of *A. japonica* trees will be discussed later. Here, we propose a model enabling estimation of the relative contribution of the sap flux–dependent and –independent components to the rate of stem $CH_4$ emission. Figure 3 shows scatter plots of the stem $CH_4$ and sap flow fluxes in September 2017 for each of the study trees. Linear regression analysis was used to determine the y-intercept corresponding to the stem $CH_4$ flux at which the sap flux becomes virtually zero. Assuming that the estimated y-axis intercept value is constant over the entire sap flux of interest, we calculated the monthly–averaged ratio of the relative contribution of the sap flux–dependent to –independent components in the stem $CH_4$ flux for each tree. The estimated relative contribution ratios over a 7-month period were found to be sample tree–dependent, with a maximum relative contribution of the sap flux-dependent component occurring around July with no more than about 11 % (Table 1). To our knowledge, no such estimate has been reported previously.

***Anatomy of fine roots***

The vascular cylinder (stele) was surrounded by a thick cortex in the primary growth root (Fig. 4A), and secondary growth gradually proceeded (Fig. 4B). The outermost layer of roots in primary growth was surrounded by ectomycorrhizal hyphae (Fig. 4A). Analysis of longitudinal sections of roots during secondary growth revealed intercellular spaces extending vertically in the cortex (Fig. 4C). We expected that such lacunae function as pathways for the diffusion of $CH_4$ in the gaseous form through the root. Cryo-SEM was used to determine whether the fine-root tissues were filled with water

(Fig. 5A and B). In the cortex, a number of large, empty (i.e., no water) intercellular spaces were observed (Fig. 5C and D). By contrast, in the endodermis, the intercellular spaces were small and filled with water (Fig. 5E and F). All parenchyma cells were filled with water and cytoplasm, whereas some xylem cells were empty in the vascular cylinder (Fig. 5G and H). Similar results were observed in all six fine-root samples analyzed (Fig. S2).

## Discussion

Year-round measurements of the $CH_4$ emission rates from the stem surfaces of *A. japonica* trees revealed the presence of a diurnal component in the emission rates, and the daytime increase in emission was found to be almost synchronous with a daytime increase in sap flux. We propose here a simple model in which the total $CH_4$ emission rate consists of "sap flux–dependent" and "sap flux–independent" components. A possible mechanism of $CH_4$ transport for the sap flux–dependent component could involve absorption of soil water containing dissolved $CH_4$ by the roots, with subsequent transport of the dissolved $CH_4$ through the conduits; volatilized $CH_4$ could then be detected with the daytime increase in the stem $CH_4$ emission rates. However, we note that the observed synchrony between $CH_4$ and sap fluxes does not exclude the possibility that the diurnal variation cannot be explained solely by sap flow. The mechanisms regulating stem $CH_4$ emission in plants remain controversial, although most previous studies have supported the primary importance of $CH_4$ transport in the gaseous form within the tree (Barba et al., 2019a). As mentioned in the introduction section, a variety of the $CH_4$ transport mechanism inside the trees have recently been suggested, for example, plant transport of soil gases is controlled by plant hydraulics as reported by Megonigal et al. (2020). Some studies have suggested that methanogen living in the heartwood could also be a source of $CH_4$ (Wang et al., 2016, 2017; Yip et al., 2018). Aside from $CH_4$ production in soil and heartwood, microbial oxidation within trees may weaken stem emissions (Jeffrey et al., 2021a; Feng et al. 2022). Clearly further investigation is needed for understanding the sap flux-depndent and -independent $CH_4$ emission mechanisms functioning in *A. japonica* trees. Our recent study (Sakabe et al., 2021)

320 suggested that, as supported by most studies for different wood species, the transport of gaseous $CH_4$
321 produced by methanogenic archaea in rhizospheric soil is primarily responsible for stem $CH_4$ emission
322 from *A. japonica* throughout the year. This conclusion was based on the following evidence: (i) stem
323 emission was observed even in winter; and (ii) stem emission was observed even during the night,
324 when the sap flow rate was nearing zero (see also Fig. 1 of this paper).

325 The ratio of the relative contribution of the sap flux–dependent and sap flux–independent
326 components, estimated based on the model proposed above, were found to vary seasonally (Table 1).
327 The sap flux–dependent component reached a maximum in summer with no more than about 11 %
328 (Table 1). It will be intriguing to consider whether the contribution ratio depends on the height of the
329 stem chamber within a given *A. japonica* tree. Measurements of the vertical profile of stem $CH_4$
330 emission from some species provided clear evidence that the stem $CH_4$ emission rates vary widely,
331 with a general trend toward decreasing $CH_4$ emission with increasing stem height for flux
332 measurements (Wang et al., 2016; Pitz & Megonigal, 2017; Barba et al., 2019b; Jeffrey et al., 2020).
333 This observation was explained by the gradual flow of gaseous $CH_4$ out of the tree and into the
334 atmosphere during transport from the roots to the upper trunk. Our preliminary measurements
335 indicated that the rate of $CH_4$ emission from *A. japonica* stems decreased with increasing height of the
336 stem flux monitoring chambers, consistent with the results of previous studies. However, the sap flux–
337 dependent component also likely depends on stem height, as $CH_4$ taken up by the roots and dissolved
338 in the sap may gradually volatilize as it moves through the tree. In addition, there is no information on
339 whether stem-height dependent microbial $CH_4$ oxidation within trees, which was evident for *M.*
340 *quinquenervia* and *C. glauca* (Jeffrey et al., 2021), are occurring in *A. japonica*. Accordingly, the
341 possibility that the contribution ratio estimated for each tree does not remain constant throughout an
342 individual tree cannot be ruled out.

343 Besides sap flow, another possible factor associated with the diurnal feature of stem $CH_4$ flux is
344 the molecular diffusivity and its temperature dependency. The coefficient of molecular diffusivity of
345 $CH_4$ in air, for example at 30 °C, is 6% larger than that at 20 °C, according to Massman (1998). The

rate of increase in diffusion coefficient seems to be comparable to the estimated contributions of diurnally varying component (Table 1). Although the gas diffusivity through wood (Sorz and Hietz, 2006) as well as stem height dependence of the relative contribution ratios need to be quantified, it would be worthwhile to examine this physical chemistry mechanisms in the future. Possible effects of temperature on diffusive transport of $CH_4$ in *Alnus glutinosa* were briefly discussed by Pangala et al (2014). Relation between air temperature or stem temperature and stem $CH_4$ flux was tested to discuss the day-night variations in $CH_4$ flux (Barba et al., 2019b; Jeffrey et al., 2020).

From the viewpoint of elucidating the $CH_4$ transport mechanism leading to the sap-dependent component, we would like to mention one more point. A closer look at the data in Figure 2 shows, there appeared to be a time lag between the daily peaks of stem $CH_4$ emission and sap flux, particularly in Tree 3 in Sep.-Oct. 2017. This observation is qualitatively similar to the results of Pitz and Megonigal (2017), in which a diurnal feature in stem $CH_4$ emission from *L. tulipifera* peaked in the late afternoon, while the sap flux reached its maximum around noon. In order to achieve a better understanding of the time lag, if existed, in *A. japonica*, $CH_4$ flux (and sap flux) with its stem height dependence should be measured at a higher temporal resolution. Furthermore, effective gas diffusivity in wood, both in axial and radial direction, and sunlight exposure conditions should also be investigated.

Our proposed model for the process of stem $CH_4$ emission in *A. japonica* suggests the primary importance of gaseous $CH_4$ transport, which can be detected as sap flow–independent emission from the stem surfaces. Therefore, in this study, we analyzed fine roots using optical and cryo-SEM to explore plant tissues that may facilitate the diffusion and transfer of gaseous $CH_4$. Tree roots take up and transport water and nutrients via their direct contact with the soil, and apical fine roots are particularly active in this process (Strock & Lynch, 2020). In this study, no lysigenous aerenchyma or secondary aerenchyma were observed in the cortex of the fine roots of *A. japonica*. However, the presence of scattered longitudinal intercellular spaces (Figs. 4 and 5) suggests that $CH_4$ in the gaseous form can be diffused from the soil to the tree stem via the roots. In addition, some xylem cells, such as vessels and fibers, were empty in the vascular cylinder of the fine roots, thereby providing a possible

372 pathway for gas diffusion. Although other researchers have speculated that anatomical features such
373 as intercellular spaces or air-filled elements in the secondary xylem could function as gas pathways in
374 waterlogging tolerance (Philipson & Coutts, 1980), our present study is the first to demonstrate this
375 phenomenon by *in situ* field observations in adult *A. japonica* trees. However, optical microscopy
376 analyses of roots of cultivated seedlings of *A. japonica* and *Salix martiana* Leyb. under experimental
377 flooding conditions suggested the formation of aerenchyma (Yamamoto et al., 1995; De Simone et al.,
378 2002). As the results of the present study were based on roots collected from the surface soil layer, it
379 will be necessary to examine the anatomic features of roots in deeper soils as well as in a variety of
380 species. Lenticels are another potential plant gas transport pathway, as they permit the entry of air
381 though the periderm (Groh et al. 2002). As many lenticels were observed in visual observations of the
382 fine-root surfaces in the present study, these structures may also play a role in gas transport. Our
383 anatomical analyses suggest that the intercellular spaces in the cortex and the empty xylem cells in the
384 fine roots of *A. japonica* could serve as passageways for the diffusive transport of gas molecules.
385 Our long-term, hourly based measurements of $CH_4$ emission from the stem surfaces of *A.*
386 *japonica* growing in a riparian wetland revealed an interesting phenomenon of diurnal variation with
387 a season-dependent amplitude. Our results provide clear evidence that a component of the rate of stem
388 $CH_4$ emission is proportional to the sap flux, allowing us to infer a possible mechanism in which $CH_4$
389 molecules dissolved in the sap are volatilized and emitted from the trunk of *A. japonica* trees. However,
390 as discussed above, there could be another mechanism which accounts for diurnally varying
391 component in stem $CH_4$ flux, and therefore observed clear association between the diurnal properties
392 in $CH_4$ flux and sap flux merits further investigation. A large portion of stem $CH_4$ emission was found
393 to be independent of sap flow, indicating that gaseous $CH_4$ molecules are also transported diffusively
394 from the rhizosphere to the tree stem. Analysis of fine roots of *A. japonica* using optical microscopy
395 and cryo-SEM suggested that intercellular spaces in the cortex and empty xylem cells could serve as
396 passageways for the diffusive transport of gas molecules.
397

**Acknowledgements**

The authors thank Ms. Y. Nambu and Ms. M. Iwasa (Kyoto University) for their technical support in the cryo-SEM experiments. The authors are grateful to the reviewers for providing us valuable comments. This work was supported in part by Grants-in-Aid for Scientific Research from the Japanese Ministry of Education, Culture, Sports, Science and Technology (18H03356 and 21H03576). This work was also supported in part by RISH, Kyoto University (Mission-linked Research), and by the Institute for Space-Earth Environmental Research, Nagoya University (Joint Research Program).

**Author Contributions**

K.T., A.S., and W.A. are equally contributing first authors who designed and led the research. K.T., A.S., and M.I. conducted flux observations. W.A. and M.T. conducted the sap flux measurements. W.A., T.I. and Y.M. conducted microscopic analyses of fine-roots. Y.K. measured micrometeorological parameters. K.T, A.S. and W.A. drafted the manuscript. All authors contributed to revision of the manuscript.

**Data availability**

The data that support the findings of this study are available from the corresponding author upon reasonable request.

**References**

**Azuma W, Ishii HR, Kuroda K, Kuroda K**. **2016**. Function and structure of leaves contributing to increasing water storage with height in the tallest *Cryptomeria japonica* trees of Japan. *Trees* **30**: 141–152.

**Barba J, Bradford MA, Brewer PE, Bruhn D, Covey K, van Haren J, Megonigal JP, Mikkelsen TN, Pangala SR., Pihlatie M, Poulter B, Rivas-Ubach A, Schadt CW, Terazawa K, Warner**

**DL, Zhang Z, Vargas R. 2019a.** Methane emissions from tree stems: a new frontier in the global carbon cycle. *New Phytologist* **222**: 18 - 28.

**Barba J, Poyatos R, Vargas R**. **2019b**. Automated measurements of greenhouse gases fluxes from tree stems and soils: magnitudes, patterns and drivers. *Scientific Reports* **9**: 1–13.

**Carmichael MJ, Bernhardt ES, Bräuer SL, Smith WK. 2014.** The role of vegetation in methane flux to the atmosphere: should vegetation be included as a distinct category in the global methane budget ? *Biogeochemistry* **119**: 1–24.

**Carmichael MJ, Helton, AM, White JC, Smith WK. 2018.** Standing dead trees are a conduit for the atmospheric flux of $CH_4$ and $CO_2$ from wetlands. *Wetlands* **38**: 133-143.

**Covey KR, Megonigal JP. 2019.** Methane production and emissions in trees and forests. *New Phytologist* **222**: 35 – 51.

**De Simone O, Müller E, Junk WJ, Schmidt W**. **2002**. Adaptations of Central Amazon tree species to prolonged flooding: Root morphology and leaf longevity. *Plant Biology* **4**: 515–522.

**Drew MC, He CJ., Morgan PW. 2000**. Programmed cell death and aerenchyma formation in roots. *Trends in Plant Science* **5**: 123-127.

**Evert RF**. **2006**. *Esau's plant anatomy: meristems, cells, and tissues of the plant body: their structure, function, and development*. New Jersey: John Wiley & Sons.

**Feng H, Guo J, Ma X, Han M, Kneeshaw D, Sun H, Malghani S, Chen H, Wang W. 2022.** Methane emissions may be driven by hydrogenotrophic methanogens inhabiting the stem tissues of poplar. *New Phytologist* **233**: 182-193.

**Gauci V, Gowing DJG, Hornibrook ERC, Davis JM, Dise NB. 2010.** Woody stem methane emission in mature wetland alder trees. *Atmospheric Environment* **44:** 2157-2160.

**Groh B, Hübner C, Lendzian KJ**. **2002**. Water and oxygen permeance of phellems isolated from trees: The role of waxes and lenticels. *Planta* **215**: 794–801.

**Itoh M, Ohte N, Koba K, Katsuyama M, Hayamizu K, Tani M. 2007.** Hydrologic effects on methane dynamics in riparian wetlands in a temperate forest catchment. *Journal of Geophysical*

*Research* **112**: G01019.

**Jeffrey LC, Maher DT, Tait DR, Euler S, Johnston SG. 2020**. Tree stem methane emissions from subtropical lowland forest (*Melaleuca quinquenervia*) regulated by local and seasonal hydrology. *Biogeochemistry* **151**: 273-290.

**Jeffrey LC, Maher DT, Chiri E, Leung PM, Nauer PA, Arndt SK, Douglas RT, Greening C, Johnston, SG. 2021a**. Bark-dwelling methanotrophic bacteria decrease methane emissions from trees. *Nature communications*, **12**: 1-8.

**Jeffrey LC, Maher DT, Tait DR, Reading MJ, Chiri E, Greening C, Johnston SG. 2021b.** Isotopic evidence for axial tree stem methane oxidation within subtropical lowland forests. *New Phytologist*, **230**: 2200-2212.

**Kirschke S, Bousquet P, Ciais P, Saunois M, Canadell JG, Dlugokencky EJ, Bergamaschi P, Bergmann D, Blake DR, Bruhwiler L et al. (48 authors) 2013**. Three decades of global methane sources and sinks. *Nature Geoscience* **6**: 813–823.

**Kosugi Y, Takanashi S, Tanaka H, Ohkubo S, Tani M, Yano M, Katayama T. 2007.** Evapotranspiration over a Japanese cypress forest. I. Eddy covariance fluxes and surface conductance characteristics for 3 years. *Journal of Hydrology* **337**: 269-283.

**Massman WJ. 1998**. A review of the molecular diffusivities of $H_2O$, $CO_2$, $CH_4$, CO, $O_3$, $SO_2$, $NH_3$, $N_2O$, NO, and $NO_2$ in air, $O_2$ and $N_2$ near STP. *Atmospheric Environment*, **32**: 1111-1127.

**Megonigal JP, Brewer PE. Knee KL. 2020.** Radon as a natural tracer of gas transport through trees. *New Phytologist* **225**: 1470-1475.

**Pangala SR, Gowing DJ, Hornibrook ERC, Gauci V. 2014.** Controls on methane emissions from Alnus glutinosa saplings. *New Phytologist* **201**: 887-896.

**Pangala SR, Hornibrook ERC, Gowing DJ. Gauci V. 2015.** The contribution of trees to ecosystem methane emissions in a temperate forested wetland. *Global Change Biology* **21**: 2642-2654.

**Pangala SR, Moore S, Hornibrook ERC, Gauci V. 2013.** Trees are major conduits for methane

egress from tropical forested wetlands. *New Phytologist* **197**: 524 - 531.

**Pangala SR., Enrich-Prast A, Basso LS, Peixoto RB, Bastviken D, Hornibrook ERC, Gatti LV, Marotta H, Calazans LSB, Sakuragui CM, Bastos WR, Malm O, Gloor E, Miller JB, Gauci V. 2017.** Large emissions from floodplain trees close the Amazon methane budget. *Nature* **552**: 230-234.

**Philipson JJ, Coutts MP**. **1980**. The tolerance of tree roots to waterlogging: Iv. Oxygen transport in woody roots of Sitka spruce and Lodgepole pine. *New Phytologist* **85**: 489–494.

**Pitz SL, Megonigal JP. 2017**. Temperate forest methane sink diminished by tree emissions. *New Phytologist* **214**: 1432-1439.

**Pitz SL, Megonigal JP, Chang C-H, Szlavecz K. 2018.** Methane fluxes from tree stems and soils along a habitat gradient. *Biogeochemistry*. **137**: 307-320.

**Purnobasuki H, Suzuki M**. **2004**. Aerenchyma formation and porosity in root of a mangrove plant, *Sonneratia alba* (Lythraceae). *Journal of Plant Research* **117**: 465–472.

**Rusch H, Rennenberg H. 1998.** Black alder (*Alnus Glutinosa* (L.) *Gaertn*.) trees mediate methane and nitrous oxide emission from the soil to the atmosphere. *Plant and Soil*. **201**: 1-7.

**Sakabe A, Kosugi Y, Okumi C, Itoh M, Takahashi K. 2016.** Impacts of riparian wetlands on the seasonal variations of watershed-scale methane budget in a temperate monsoonal forest. *Journal of Geophysical Research: Biogeosciences* **121**: 1717-1732.

**Sakabe A, Takahashi K, Azuma W, Itoh M, Tateishi M, Kosugi Y. 2021.** Seasonal variation and controlling factors of stem methane emissions from *Alnus japonica* in a riparian wetland of a temperate Forest. *Journal of Geophysical Research: Biogeosciences* **126**: e2021JG006326.

**Saunois M, Stavert AR, Poulter B, Bousquet P, Canadell JG, Jackson RB, Raymond PA, Dlugokencky EJ, Houweling S, Patra PK et al. (total 91 authors) 2020.** The Global Methane Budget 2000-2017. *Earth System Science Data* **12**: 1561–1623.

**Schindler T, Machacova K, Mander Ü, Escuer-Gatius J, Soosaar K. 2021**. Diurnal tree stem $CH_4$ and $N_2O$ flux dynamics from a riparian alder forest. *Forests* **12**: 863 (9 pages).

**Sorz J and Hietz P. 2006**. Gas diffusion through wood: implications for oxygen supply. *Trees* **20**: 34-41.

**Stevens KJ, Peterson RL, Reader RJ**. **2002**. The aerenchymatous phellem of Lythrum salicaria (L.): A pathway for gas transport and its role in flood tolerance. *Annals of Botany* **89**: 621–625.

**Strock CF, Lynch JP**. **2020**. Root secondary growth: an unexplored component of soil resource acquisition. *In: van Dongen J., Licausi F. (eds) Low-Oxygen Stress in Plants.* Plant Cell Monographs, vol 21. Springer, Vienna. https://doi.org/10.1007/978-3-7091-1254-0_13.

**Takahashi H, Yamauchi T, Colmer TD, Nakazono M**. **2014**. Aerenchyma Formation in Plants. *Annals of Botany* **126**: 205–218.

**Terazawa K, Ishizuka S, Sakata T, Yamada K, Takahashi M. 2007.** Methane emissions from stems of *Fraxinus mandshurica* var. *japonica* trees in a floodplain forest, *Soil Biology and Biochemistry* **39**: 2689-2692.

**Terazawa K, Tokida T, Sakata T, Yamada K, Ishizuka S. 2021.** Seasonal and weather-related controls on methane emissions from the stems of mature trees in a cool-temperate forested wetland. *Biogeochemistry* **156**: 211–230.

**Terazawa K, Yamada K, Ohno Y, Sakata T, Ishizuka S. 2015.** Spatial and temporal variability in methane emissions from tree stems of Fraxinus mandshurica in a cool-temperate floodplain forest, *Biogeochemistry* **123**: 349–362.

**Verboven P, Pedersen O, Herremans E, Ho QT, Nicolaï BM, Colmer TD, Teakle N**. **2012**. Root aeration via aerenchymatous phellem: Three-dimensional micro-imaging and radial O2 profiles in Melilotus siculus. *New Phytologist* **193**: 420–431.

**Wang ZP, Gu Q, Deng FD, Huang JH, Megonigal JP, Yu Q, Lü XT, Li, LH, Chang S, Zhang YH, Feng JC, Han XG. 2016.** Methane emissions from the trunks of living trees on upland soils, *New Phytologist* **211**: 429-439.

**Wang ZP, Han SJ, Li HL, Deng FD, Zheng, YH, Liu HF, Han XG. 2017.** Methane production explained largely by water content in the heartwood of living trees in upland forests. *Journal of Geophysical Research: Biogeosciences* **122**: 2479–2489.

**Webb J, Jackson MB**. **1986**. A transmission and cryo-scanning electron microscopy study of the formation of aerenchyma (cortical gas-filled space) in adventitious roots of rice (*Oryza sativa*). *Journal of Experimental Botany* **37(179)**: 832–841.

**Yamamoto F, Sakata T, Terazawa K**. **1995**. Growth, morphology, stem anatomy, and ethylene production in flodded *Alnus japonica* seedlings. *IAWA Journal* **16(1)**: 47–59.

**Yamauchi T, Shimamura S, Nakazono M, Mochizuki T**. **2013**. Aerenchyma formation in crop species: A review. *Field Crops Research* **152**: 8–16.

**Yip DZ, Veach AM, Yang ZK, Cregger MA, Schadt CW. 2018.** Methanogenic Archaea dominate mature heartwood habitats of Eastern Cottonwood (Populus deltoides). *New Phytologist* **222**: 115–121.

**Supporting Information**

**Fig. S1** Cryo-SEM images of fine roots of *A. japonica* sapling grown in the laboratory under well-watered conditions.

**Fig. S2** Optical and cryo-SEM images of fine roots of *A. japonica* trees.

**Table 1**: Ratios of the relative contribution of sap flux–dependent to sap flux–independent components in the rates of $CH_4$ emission from the stem surfaces of *Alnus japonica* trees: sap flux–dependent component / sap flux–independent component. Values in parentheses indicate the coefficient of determination for regression ($p < 0.01$), as typically shown in Figure 3 (see main text for details).

| **Observed Month/year** | **Tree 1** | **Tree 2** | **Tree 3** |
|---|---|---|---|
| Sept 2017 | 2.7% (0.90) | 3.8% (0.92) | 8.7% (0.78) |
| Oct 2017 | 1.5% (0.26) | 1.7% (0.36) | 4.2% (0.41) |
| Nov 2017 | 2.0% (0.41) | 1.0% (0.29) | 2.2% (0.44) |
| May 2018 | 3.1% (0.75) | 3.7% (0.77) | N/A* |
| June 2018 | 3.4% (0.84) | 5.6% (0.86) | 10.2% (0.87) |
| July 2018 | 4.1% (0.89) | N/A* | 12.2% (0.62) |
| Aug 2018 | 3.3% (0.87) | 2.8% (0.33) | 9.7% (0.75) |

*N/A: not estimated due to lack of sap flux data.

553 **Figure captions**

554 **Figure 1**: $CH_4$ flux from the stem surfaces of three *Alnus japonica* trees in (A) September 9-16, 2017,
555 and (B) July 11-18, 2018, together with sap flux, downward short-wave radiation (denoted as S↓), air
556 temperature, and rainfall (bar graph). Both periods in figure 1a and 1b are leafy season. Measurements
557 of $CH_4$ flux and sap flux were conducted with 1-h resolution (see main text for details). Sap flux data
558 for Tree 2 in (B) were not available due to unavoidable circumstances. Red, Tree 1; blue, Tree 2; green,
559 Tree 3. No rainfall was observed in July 11-18, 2018.
560
561 **Figure 2**: Monthly average stem $CH_4$ flux and sap flux for three *Alnus japonica* trees for September
562 to November 2017 and May to July 2018; diurnal data with 1-h resolution were averaged over each
563 month. Shaded ranges represent 95% CI. Data were excluded when the cumulative rainfall in the
564 previous 24 h exceeded 10 mm. Color codes are the same as indicated in the legend for Figure 1. The
565 sap flux data for Tree 1 in May 2018 and for Tree 3 in July 2018 were not available due to instrument
566 malfunction.
567
568 **Figure 3**: Plots of correlation between $CH_4$ flux and sap flux for three *Alnus japonica* trees in
569 September 2017, using the data shown in Figure 2. Each graph has 24 data points, each of which is an
570 hourly one-month average corresponding to the data shown in Figure 2 (mean and 95% CI). The
571 determination coefficients for regression were 0.89, 0.93, and 0.84 for Tree 1, Tree 2, and Tree 3,
572 respectively ($p < 0.01$). The y-axis intercepts correspond to the stem $CH_4$ fluxes at which the sap fluxes
573 become virtually zero and were assumed to indicate the contribution of the diurnally unvarying
574 component of $CH_4$ emission from the stem surface. The estimated y-axis intercept value was subtracted
575 from the observed $CH_4$ flux values, whose output was integrated over the range of the observed sap
576 flux, thereby the contribution of the diurnally varying component could be calculated (See main text
577 for details).
578

579

580 **Figure 4**: Optical microscopy images of the fine-root anatomy of *A. japonica* trees. Transverse
581 sections were double stained with safranin-fast green to indicate roots in primary growth (A) and
582 secondary growth (B). Intercellular spaces (indicated by arrows) extended vertically in the cortex of a
583 longitudinal section double stained with safranin-fast green of a secondary growth root (C).

584

585 **Figure 5**: Optical and cryo-SEM images of fine roots of Japanese *A. japonica* trees. Transverse surface
586 of a root in primary growth observed by optical microscope (A) and cryo-SEM (B). Panel C–H are
587 magnified images corresponding to the rectangle-denoted areas in panel B. Large, empty (i.e., no
588 water) intercellular spaces were observed in the cortex (C, D). Intercellular spaces (arrows) were small
589 and filled with water (frozen) in the endodermis (E, F). All parenchyma cells were filled with water,
590 whereas some xylem cells were empty (i.e., no water) in the vascular cylinder (G, H).

591

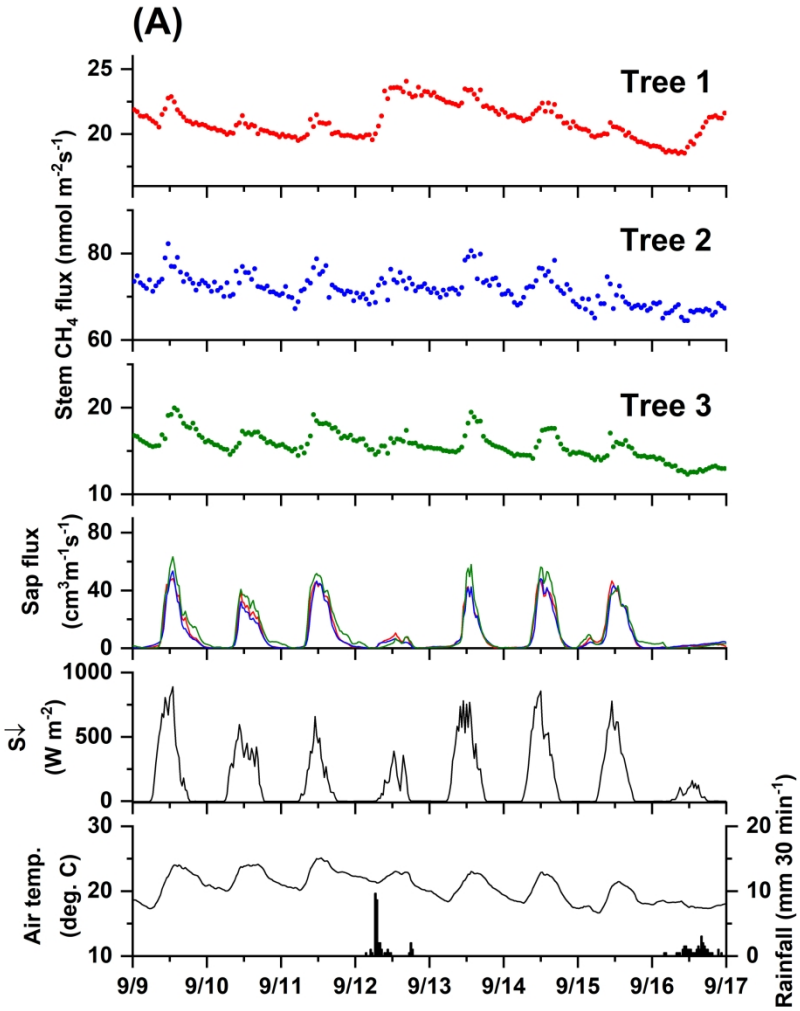


Fig. 1A

209x296mm (300 x 300 DPI)

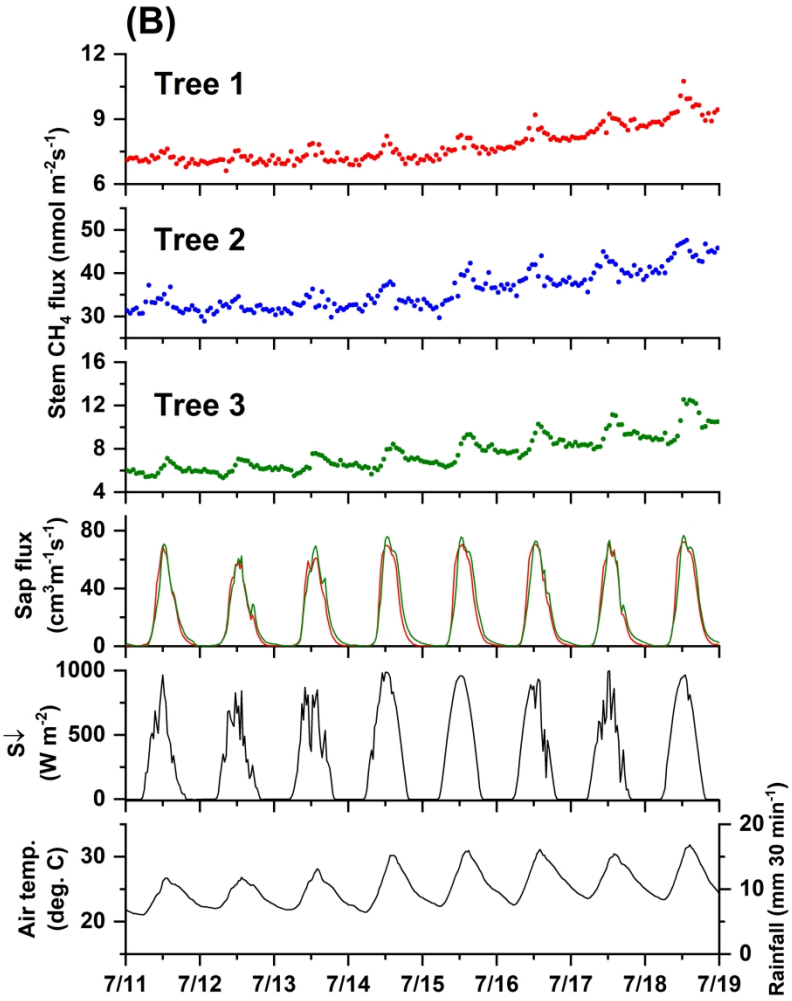


Fig. 1B

209x296mm (300 x 300 DPI)

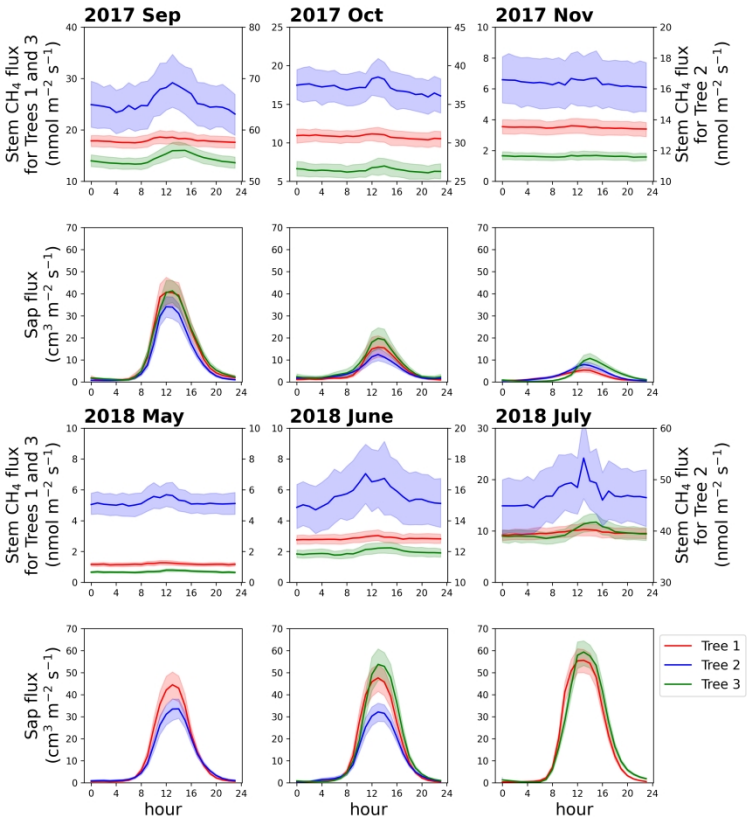


Fig. 2

1190x1190mm (96 x 96 DPI)

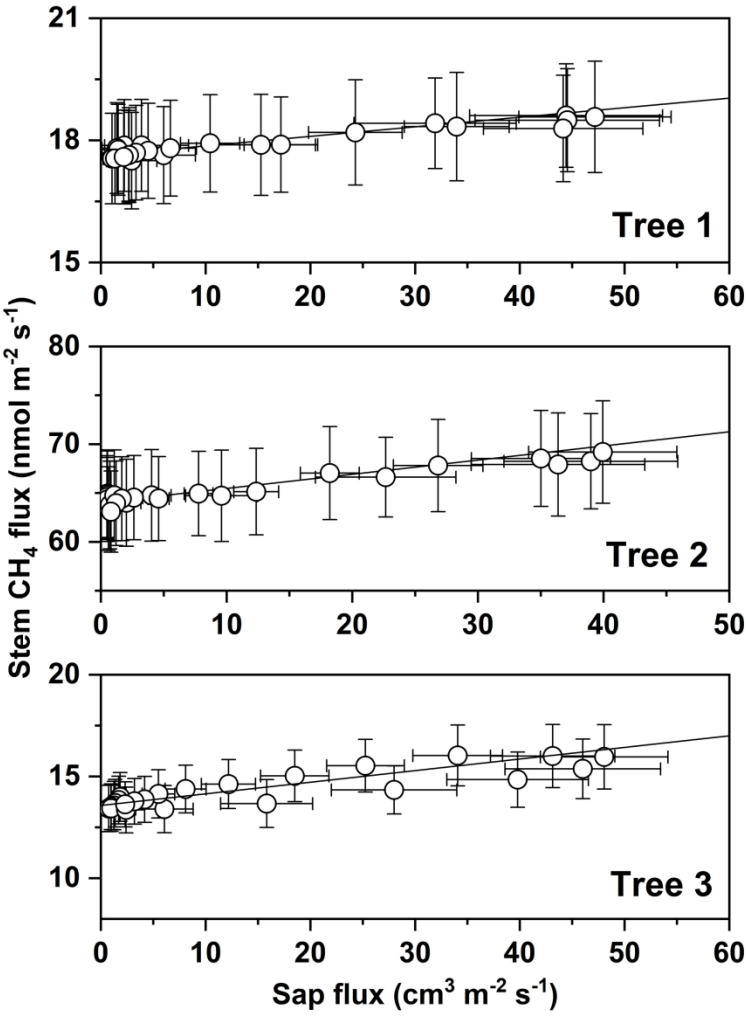


Fig 3

202x289mm (300 x 300 DPI)

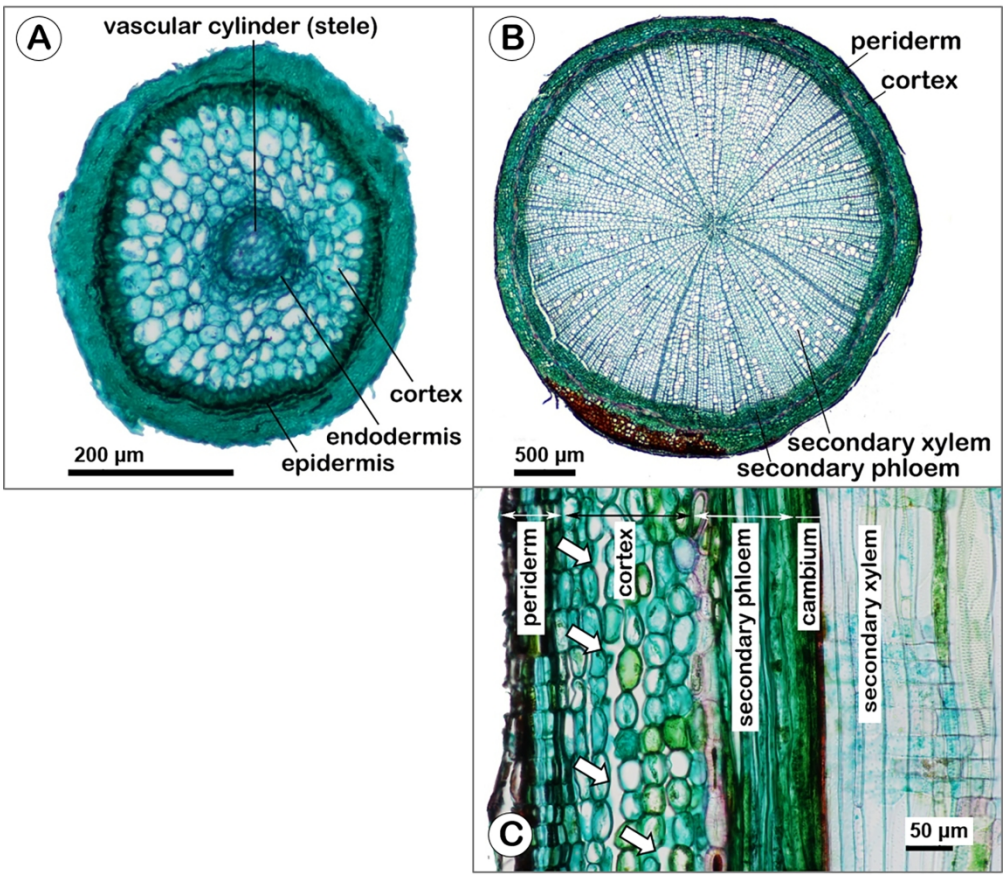


Fig. 4

181x158mm (300 x 300 DPI)

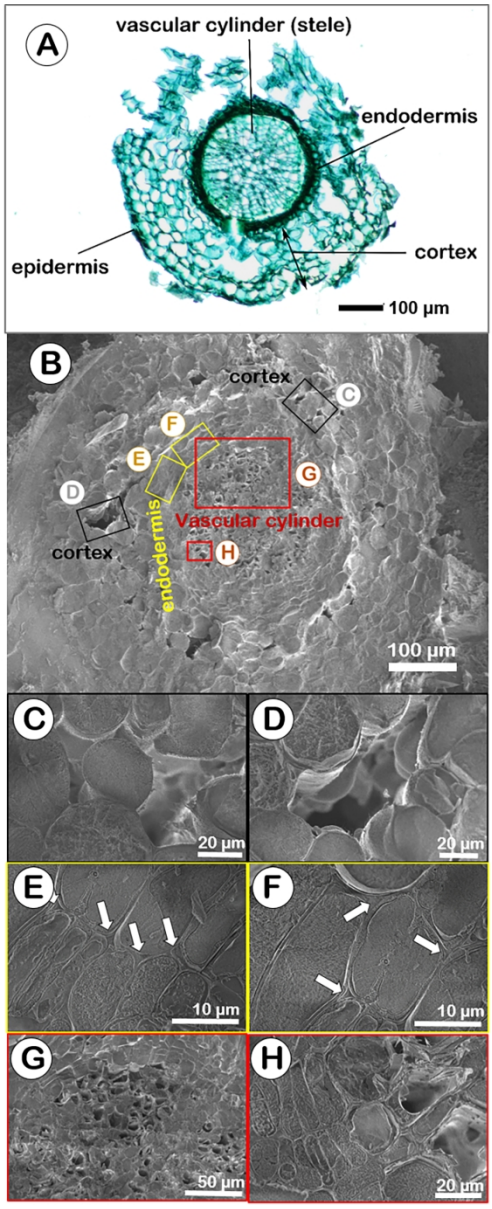


Fig. 5

98x235mm (300 x 300 DPI)

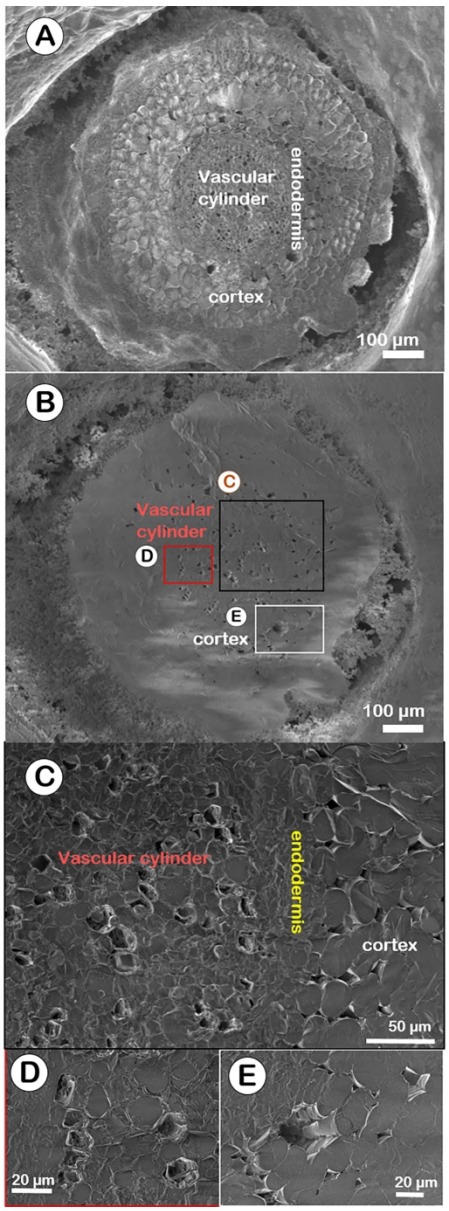


Fig. S1

99x259mm (300 x 300 DPI)

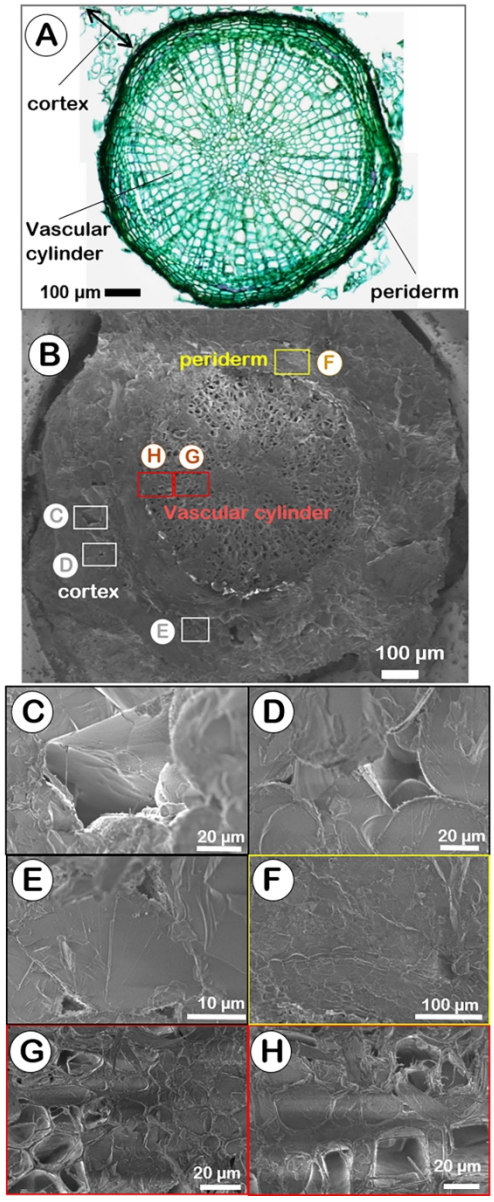


Fig. S2

98x234mm (300 x 300 DPI)